ACS APPLIED MATERIALS & INTERFACES

Research Article

www.acsami.org

One-Dimensional Porphyrin Nanoassemblies Assisted via Graphene Oxide: Sheetlike Functional Surfactant and Enhanced Photocatalytic Behaviors

Peipei Guo,[†] Penglei Chen,*[,†,‡] and Minghua Liu*[,†]

[†]Beijing National Laboratory for Molecular Science, CAS Key Laboratory of Colloid, Interface and Chemical Thermodynamics, Institute of Chemistry, Chinese Academy of Sciences, No. 2 Zhongguancun Beiyijie, Beijing 100190, P. R. China

[‡]College of Chemistry and Molecular Engineering, Zhengzhou University, 100 Science Road, Zhengzhou, Henan 450001, P. R. China

Supporting Information

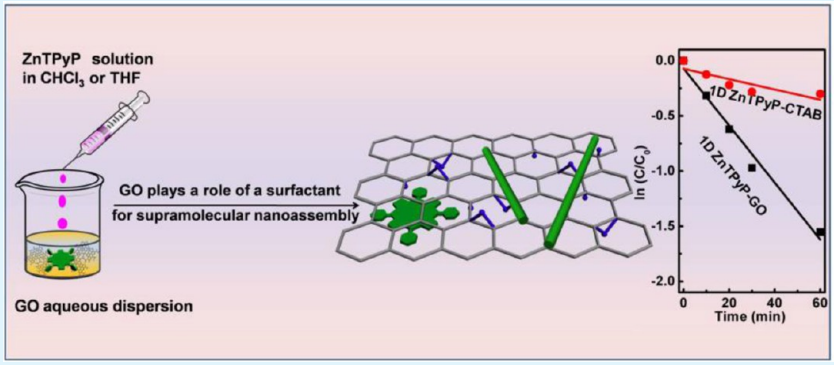

ABSTRACT: Surfactant-assisted self-assembly (SAS) has received much attention for supramolecular nanoassemblies, due to its simplicity and easiness in realizing a controllable assembly. However, in most of the existing SAS protocols, the employed surfactants work only as a regulator for a controllable assembly but not as active species for function improvement. In this paper, we report that a porphyrin, zinc 5,10,15,20-tetra(4-pyridyl)-21H,23H-porphine (ZnTPyP), could be assembled to form one-dimensional (1D) supramolecular nanostructures via a SAS method, wherein graphene oxide (GO) plays a fascinating role of sheetlike surfactant. We show that, when a chloroform or tetrahydrofuran solution of ZnTPyP is injected into an aqueous dispersion of GO, 1D supramolecular nanoassemblies of ZnTPyP with well-defined internal structures could be easily formulated in a controllable manner. Our experimental facts disclose that the complexation of ZnTPyP with the two-dimensional GO nanosheets plays an important role in this new type of SAS. More interestingly, compared with the 1D ZnTPyP nanoassemblies formulated via a conventional SAS, wherein cetyltrimethylammonium bromide is used as surfactant, those constructed via our GO-assisted SAS display distinctly enhanced photocatalytic activity for the photodegradation of rhodamine B under visible-light irradiation. Our new findings suggest that GO could work not only as an emergent sheetlike surfactant for SAS in terms of supramolecular nanoassembly but also as functional components during the performance of the assembled nanostructures.

KEYWORDS: *graphene oxide, sheetlike surfactant, supramolecular nanoassemblies, surfactant-assisted self-assembly, porphyrin*

1. INTRODUCTION

Self-assembly (SA), which can occur in synthetic and natural systems and can lead to the formation of a variety of ordered structures at various levels, is a ubiquitous principle in nature.[1−5] Currently, SA is considered to be an effective bottom-up protocol for supramolecular nanostructures.[6−15] A paramount of supramolecular nanoassemblies has been constructed via diverse SA strategies,[6−15] wherein those via surfactant-assisted self-assembly (SAS) have received particular attention.[16−24] This is owing to its inherent easiness in realizing a controllable assembly by tuning the concentration of surfactants or selecting various surfactants with distinct properties.[16−30] Thus far, numerous inorganic-based nanostructures have been formulated via SAS,[26−30] while the paradigms concerning the organic-based supramolecular nanomaterials are relatively fewer; although compared with their inorganic counterparts, supramolecular nanostructures with regard to organic building blocks have, in particular, fascinated scientists owing to their solution processability and considerable variety and flexibility in molecular design.[6−24,31−34] Practically, a crucial issue of SAS is to select or design appropriate surfactants to assist the assembly. Wide varieties of anionic, cationic, nonionic, amphoteric/zwitterionic, and polymeric surfactants, which are geometrically featured with a

Received: April 7, 2013
Accepted: May 7, 2013
Published: May 7, 2013

Scheme 1. Chemical Structure of ZnTPyP (A) and GO (B). (C) Schematic Illustration for our GO-Based SAS and a Plausible Explanation for the Controlled Assembly of ZnTPyP 1D Supramolecular Nanoassemblies via Our SAS[a]

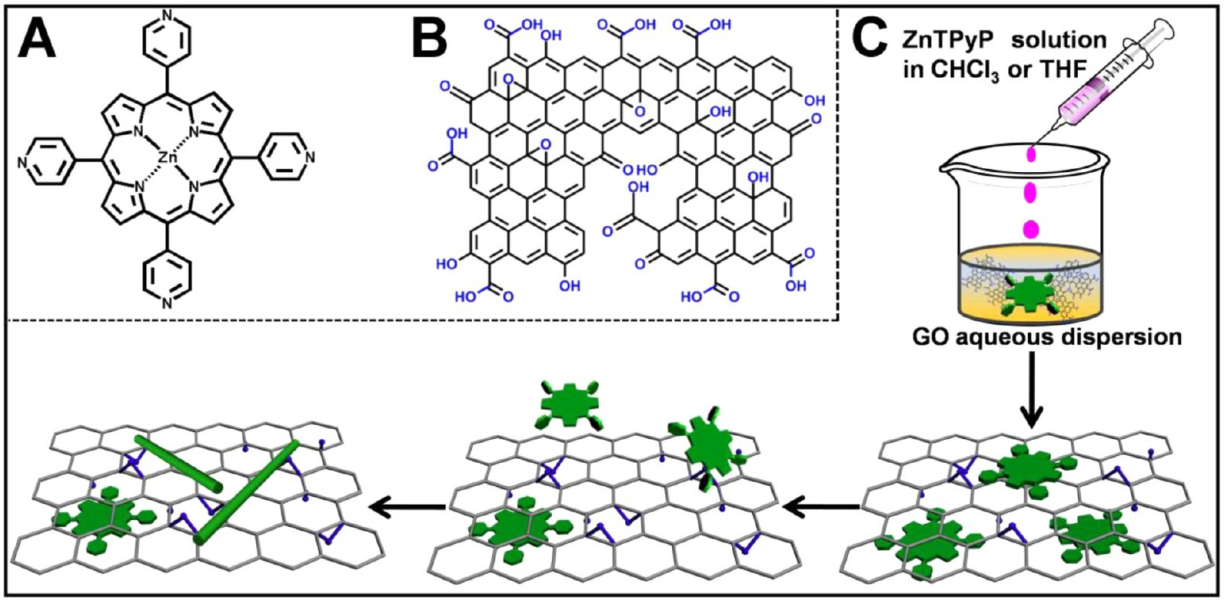

[a]The drawings are not to scale.

tadpole, bola-, gemini, linear configuration, have been employed for SAS.[16−30] Nevertheless, it is still a subject of paramount importance to develop new type surfactants to initiate new platforms for supramolecular nanoassemblies in terms of SAS.

Recently, organic-based supramolecular nanoassemblies in terms of porphyrin building blocks have been attracting great interest due to their potential application possibilities in various fields of general concern.[35,36] Especially, they play many critical roles in the biological systems, such as oxygen transport, enzymatic catalysis, and light-harvesting.[35,36] Some of the functions of porphyrins are strongly related to their supramolecular assemblies.[37] For example, in natural photosynthetic systems, chlorophyll, a porphyrin analogue, is often self-organized into nanoscale suprastructures, by which they perform many of the light-harvesting and energy/electron transferring functions.[38−40] Therefore, it is an issue of paramount importance to control the assembly of porphyrins. Thus far, several porphyrin-based supramolecular nanostructures have been successfully assembled via SAS protocol, wherein conventional surfactants are employed for a controllable assembly.[16−24] For instance, we have recently reported a controllable assembly of zinc 5,10,15,20-tetra(4-pyridyl)-21*H*,23*H*-porphine (ZnTPyP, Scheme 1A) via a SAS by using cetyltrimethylammonium bromide (CTAB) as surfactant.[17] However, in most of the existing SAS for porphyrin nanoassemblies,[16−24] the employed surfactants work only as a regulator for a controllable assembly but not as active species for function improvement. Accordingly, it is strongly desired to find functional surfactants not only for a controllable assembly but also for a function enhancement.

Recently, graphene oxide (GO) has received much attention as a novel cousin of graphene.[41−48] Geometrically (Scheme 1B), GO could be figured as graphene fragment, whose edge is mainly decorated with carbonyl and carboxyl groups, and basal plane with epoxide and hydroxyl groups. This endows GO with amphiphilicity, where the periphery is inclined to be hydrophilic, while the center is hydrophobic. By virtue of this feature, it is proved that GO could display interfacial activities, work as dispersing agent, or generate Pickering emulsions, all of which behave like an intriguing 2D sheetlike surfactant.[44−48] These new facets of GO might inspire new discoveries in scientific communities.[44−48] However, to our knowledge, there might be no earlier report using GO as surfactant to fulfill SAS for the construction of supramolecular nanostructures, although an investigation on this issue might launch a new bright future not only for GO but also for SAS.

We report herein our new findings that ZnTPyP could be organized to form one-dimensional (1D) supramolecular nanoassemblies with well-defined internal structures via a SAS method, wherein GO plays a role of a sheetlike surfactant. We show that, by adding a chloroform (oil, viz., water-immiscible solvent) or tetrahydrofuran (THF, water-miscible solvent) solution of ZnTPyP into an aqueous dispersion of GO (Scheme 1C), 1D supramolecular nanostructures of ZnTPyP, whose length depends on the concentration of GO, could be controllably assembled. It is revealed that the complexation of ZnTPyP with the two-dimensional GO nanosheets plays an important role in this kind of GO-assisted SAS. Interestingly, compared with the 1D ZnTPyP nanoassemblies formulated via a conventional SAS, wherein cetyltrimethylammonium bromide (CTAB) is used as surfactant, those constructed via our GO-assisted SAS display distinctly enhanced photocatalytic activity for the photodegradation of rhodamine B (RhB) under visible-light irradiation. Our investigation discloses a brand-new aspect of GO nanosheets in terms of supramolecular nanoassembly. We believe that this might provide GO with new opportunities in the interdisciplinary area of supramolecular assembly, porphyrin engineering, nanofabrication, and material science.

2. MATERIALS AND METHODS

2.1. Materials. Zinc 5,10,15,20-tetra(4-pyridyl)-21*H*,23*H*-porphine (ZnTPyP, Aldrich), cetyltrimethylammonium bromide (CTAB, Aldrich), and graphite power (Alfa Aesar, 325 mesh, 99.9995%) were used as received without further purification or treatment. Other

chemicals, including H_2SO_4 (98%), $KMnO_4$ (99.5%), $NaNO_3$ (99%), HCl (36−38%), $BaCl_2$ (99.5%), and H_2O_2 (~30%), which were used for the synthesis of GO nanosheets, were purchased from Beijing Chemical Co., Ltd. and used without further treatment. Distilled chloroform and THF were used as solvent for ZnTPyP, and Milli-Q water (18 MΩ cm) was used as solvent for GO and for CTAB.

2.2. Preparation of GO Nanosheets. GO nanosheets were formulated via a chemical exfoliation of the graphite powder using a modified Hummers method.[49,50] Experimentally, graphite powder (1 g) was added to concentrated H_2SO_4 (0 °C, 23 mL). Then, $NaNO_3$ (0.5 g) and $KMnO_4$ (3 g) was added gradually to the system successively under vigorous magnetic stirring. During this procedure, the temperature of the mixture was maintained below 20 °C using an ice bath. After that, the mixture was stirred at 35 °C for 30 min. Subsequently, ultrapure Milli-Q water (46 mL) was added to the system slowly, and the temperature of the system was increased to 98 °C. The mixture was maintained at 98 °C for 15 min. To terminate the reaction, ultrapure Milli-Q water (140 mL) was added to the reaction system, after which H_2O_2 (10 mL, 30%) solution was added. The solid product was separated by centrifugation and washed repeatedly with HCl solution (5%) until sulfate could not be detected by $BaCl_2$. The obtained samples were dried in a vacuum oven at 65 °C overnight. To obtain aqueous dispersion of GO nanosheets, the synthesized solid product (100 mg) was added to ultrapure Milli-Q water (50 mL), after which the system was treated with an ultrasonic homogenizer (Ningbo Scientz Biotechnology Co., Ltd., Scientz-II D; frequency: 20 kHz; output power: 400 W) for 1 h. Subsequently, the suspension was repeatedly treated by high-speed centrifugation (8000 rpm, 5 min) for four times to remove impurities. The mass concentration of the obtained aqueous dispersion of GO nanosheet was estimated to be 1 mg mL^{-1}. Thus-obtained aqueous dispersion of GO nanosheets was diluted to the desired concentration with Milli-Q water when used as the host solution for SAS.

2.3. Assembly of ZnTPyP Supramolecular Nanostructures via GO-Assisted SAS. The assembly of ZnTPyP supramolecular nanostructures was carried out using an aqueous dispersion of GO nanosheets of different concentrations (0, 0.01, 0.02, or 0.1 mg mL^{-1}) as host solution and a solution of ZnTPyP dissolved in chloroform or THF (2×10^{-4} M) as guest solution. The samples are designated as chloroform/water system and THF/water system, respectively, when a chloroform or THF solution of ZnTPyP was employed as guest solution.

Typically, in the case of the chloroform/water system, an 800 μL aliquot of ZnTPyP solution was injected into a 10 mL aqueous dispersion of GO nanosheets under vigorous magnetic stirring, soon after which an opaque dispersion was obtained. A transparent yellowish dispersion was produced after the vigorous stirring was maintained for 20 min for the evaporation of chloroform. Subsequently, the UV−vis spectra of the dispersions were measured. The produced nanoassemblies were obtained by centrifugation (10 000 rpm, 15 min), and the precipitates were collected and redispersed in Milli-Q water, after which the solution was again subjected to centrifugation. These operations were performed 3 times repeatedly. These operations were carried out to condense the obtained nanostructures such that the related measurements of characterizations could be performed easily and efficiently. The final products were characterized by means of scanning electron microscopy (SEM), low-resolution transmission electron microscopy (LRTEM), high-resolution transmission electron microscopy (HRTEM), fast Fourier transformation (FFT), and X-ray diffraction (XRD). On the other hand, the nanostructures could also be obtained by filtering on a Millipore filter (pore size 200 nm), after which the samples were characterized by the above-mentioned methods. Practically, we found that similar results were obtained for the samples produced by centrifugation and filtration.

In the case of the THF/water system, similar operations were carried out, except that the assembly system manifests itself as a transparent dispersion all the time throughout the SAS period. This is owing to the nice miscibility between THF and water, which experimentally permits us to monitor the SAS via real-time UV−vis spectra and SEM. In this case, to terminate the assembly at an appointed time, the nanostructures were obtained by filtering on the Millipore filter and washed adequately with Milli-Q water.

2.4. Assembly of 1D ZnTPyP Supramolecular Nanostructures via CTAB-Assisted SAS. Besides the above-mentioned nanofabrications, the 1D supramolecular nanoassemblies of ZnTPyP were also formulated using a conventional SAS protocol, wherein CTAB was employed as surfactant. The detailed process for the synthesis is the same as that described previously.[51]

2.5. Photocatalytic Performance. In a typical photocatalytic experiment, a 250 μL aqueous solution of RhB with an extremely high concentration (400 mg L^{-1}) was dispersed in a 10 mL aqueous dispersion of the ZnTPyP nanoassemblies constructed by means of GO-assisted or CTAB-assisted SAS protocols, wherein the initial concentration of RhB in the catalytic systems was estimated to be ca. 10 mg L^{-1}. The dispersion was kept in the dark for 30 min for the dark adsorption experiment, after which the photodegradation was carried out under visible light irradiation. The dark adsorption time was designed to be 30 min because it was found that, when a longer adsorption time, for example 36 h, was employed, similar results were obtained. The light source for the photocatalytic experiment was a 500 W xenon arc lamp installed in a laboratory lamp housing system (CHF-XM35-500 W, Beijing Trusttech Co. Ltd., China). Before entering the photocatalytic reactor, the light passed through a 10 cm water filter and a UV cutoff filter (>400 nm). During the photodegradation, aliquots of dispersion (0.4 mL) were taken out from the reaction system at an appointed time for real-time sampling. To evaluate the photocatalytic activities, C is the concentration of RhB molecules at a certain real-time t, and C_0 is that of the RhB solution immediately before it is kept in the dark. The catalytic performances were also carried out using our original GO nanosheets, the ZnTPyP/GO complexes formulated at a high concentration of GO (0.1 mg mL^{-1}), and the commercially available P25−TiO_2, as catalysts. For comparison, blank experiments without catalyst were also performed under the similar experimental conditions.

The rate constant of the photocatalytic reaction was deduced by a kinetic linear simulation of the experimentally obtained curve of photocatalytic activity. The detailed method for the kinetic linear simulation is the same as that described previously.[52,53]

2.6. Electrochemical Impedance Spectral (EIS) Measurements. The EIS measurements were performed on a Solartron 1255B frequency response analyzer and a Solartron SI 1287 electrochemical interface system by using three-electrode cells. The film electrodes of the 1D ZnTPyP nanostructures assisted by GO or CTAB served as the working electrode, with a platinum wire as the counter electrode and a Ag/AgCl (saturated KCl) electrode as the reference electrode. The measurement was carried out in the presence of a 2.5 mM $K_3[Fe(CN)_6]/K_4[Fe(CN)_6]$ (1:1) mixture as a redox probe in 0.1 M KCl solution. The impedance spectra were recorded with the help of ZPlot/ZView software under an ac perturbation signal of 10 mV over the frequency range of 1 MHz to 100 mHz.

2.7. Apparatus and Measurements. The SEM measurements were carried out using a Hitachi S-4800 system (Japan). Nearly 30 nm of platinum was deposited on the sample surface by vacuum deposition to obtain SEM images with good contrast. XRD measurements were performed on a PANalytical X'Pert PRO instrument with Cu $K\alpha$ radiation. A JASCO UV-550 spectrophotometer was used for the measurements of UV−vis spectra. LRTEM and HRTEM images of the nanomaterials were obtained with a FEI Tecnai G^2 F20 U-TWIN, which was operated with an accelerating voltage of 80 kV. The accelerating voltage was set as 80 kV, because during the measurements of the HRTEM images, our supramolecular nanostructures suffer a fast amorphization under a stronger electron beam (acceleration voltage of 200 kV).[17] The Raman spectra were recorded on a Renishaw inVia plus Raman microscope using a 514.5 nm argon ion laser. The EIS measurements were performed on a Solartron 1255B frequency response analyzer and a Solartron SI 1287 electrochemical interface system by using three-electrode cells. All the measurements were carried out at room temperature.

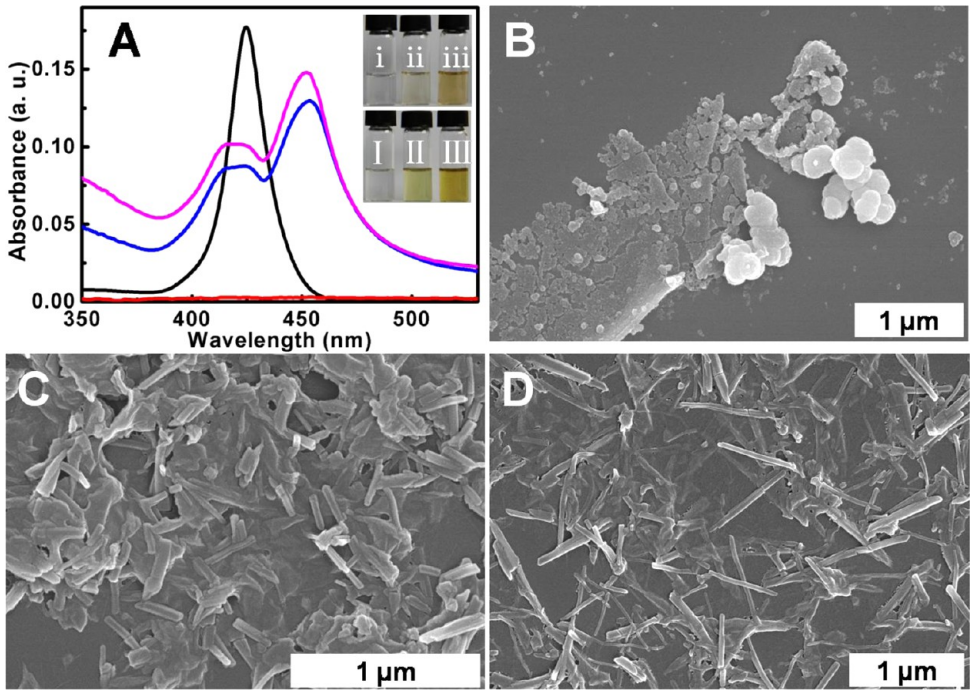

Figure 1. A): UV−vis spectra of Sample (0) (red curve), Sample (0.01) (blue curve), and Sample (0.02) (magenta curve) assembled in the chloroform/water system. That of ZnTPyP dissolved in chloroform solution (black curve) is also presented for comparison. Inset in panel (A): digital photographs of aqueous dispersions of the original GO nanosheets with a concentration of 0 (i), 0.01 (ii), and 0.02 (iii), and those of the Sample (0) (I), Sample (0.01) (II), and Sample (0.02) (III). SEM images of Sample (0) (B), Sample (0.01) (C), and Sample (0.02) (D) fabricated in the chloroform/water system.

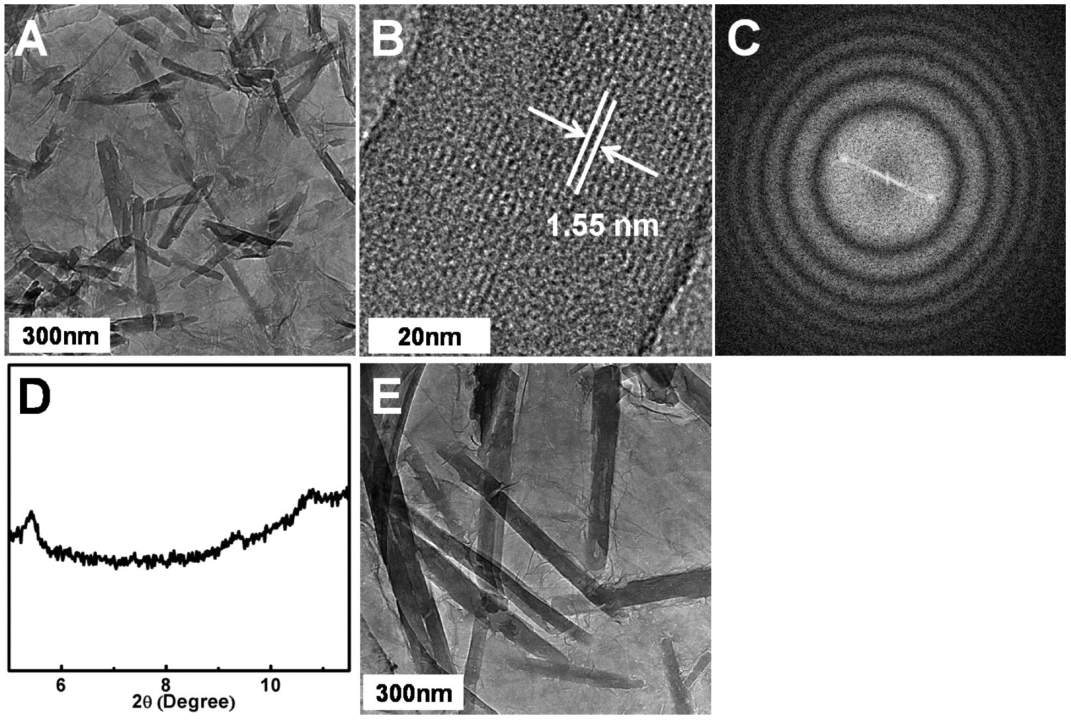

Figure 2. LRTEM image (A), HRTEM image (B), FFT pattern (C), and XRD pattern (D) of Sample (0.01) and LRTEM image of sample (0.02) (E), which are assembled in a chloroform/water system.

3. RESULTS AND DISCUSSION

3.1. Assembly and Characterization of One-Dimensional ZnTPyP Supramolecular Nanostructures via GO-Assisted SAS. For a typical assembly, an oil solution of ZnTPyP dissolved in chloroform (guest solution) was injected into an aqueous dispersion of GO (host solution) of different concentration under vigorous stirring at room temperature. The stirring was maintained for 20 min for the evaporation of chloroform, after which the UV−vis spectra of the resultant dispersion were investigated (designated as chloroform/water

dx.doi.org/10.1021/am401260n | ACS Appl. Mater. Interfaces 2013, 5, 5336−5345

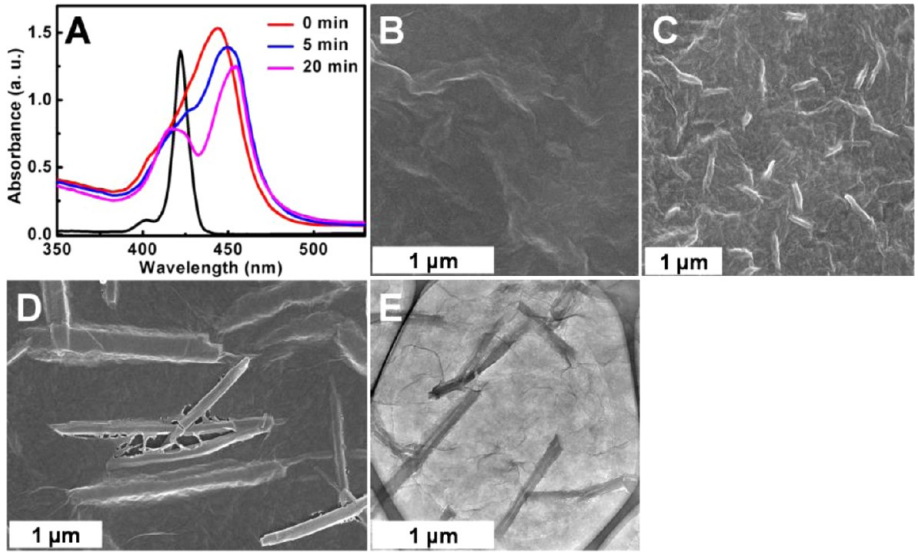

Figure 3. (A) Real-time UV−vis spectra of Sample (0.02) assembled in THF/water system as a function of the stirring time. That of ZnTPyP dissolved in THF solution (black curve) is also presented for comparison. The SEM images of the corresponding samples assembled with a stirring time of 0 (B), 5 (C), and 20 (D) min. (E) The LRTEM image of the nanoassemblies shown in panel D.

system, hereafter). Practically, when the concentration of GO aqueous dispersion is 0 mg mL^{-1} (viz. plain water, thus-obtained samples are designated as Sample (0), hereafter), purple aggregates, either floating on the surface of the dispersion or adsorbed on the wall of the flask or on the stirring rod, are obtained after the evaporation of chloroform, while the dispersion itself is nearly colorless like plain water (Figure 1A, inset). These observations suggest that ZnTPyP could hardly be introduced into plain water by chloroform. This is reasonable, since chloroform is immiscible with water, and ZnTPyP is nearly a water insoluble compound. This could be verified by the UV−vis spectrum of thus-obtained dispersion, where only negligible absorptions are observed, while that of the chloroform solution of ZnTPyP displays a distinct B-band at 425 nm (Figure 1A). Nevertheless, the purple aggregates of ZnTPyP adsorbed on the stirring rod could be scraped off and subjected to SEM measurements. Irregular species could be observed from the SEM image of such aggregates (Figure 1B), indicating that ZnTPyP could not be organized to form well-defined supramolecular nanoassemblies when plain water is employed as host solvent.

Interestingly, when an aqueous dispersion of GO with a concentration of 0.01 mg mL^{-1} was used as host solution (designated as Sample (0.01), hereafter), an opaque dispersion was obtained immediately after the injection of the chloroform solution of ZnTPyP. This observation indicates that, with the presence of GO nanosheets, chloroform, an oil phase which is generally immiscible with plain water, could be introduced into the aqueous system, basically suggesting that GO nanosheets could play a role of surfactant in the dispersion.[17] After the evaporation of chloroform, a transparent dispersion, whose color became deepened yellowish compared with the original GO host solution (Figure 1A, inset), was obtained. The UV−vis spectrum of this dispersion shown in Figure 1A indicates that besides a weak B-band at ca. 425 nm, two B-bands at ca. 415 nm and ca. 455 nm are also evidently detected. Compared with the monomeric ZnTPyP B-band at ca. 425 nm, these two bands exhibit distinct bathochromic and hypsochromic shifts, respectively, suggesting that most of the ZnTPyP units form well-defined J-type supramolecular assemblies.[51,54−57] The former and latter B-band could be ascribed to the transition moments parallel and perpendicular to the aggregate axis, respectively.[51,54−57] These results imply that, with the assistance of GO nanosheets, ZnTPyP could be organized to form well-defined supramolecular assemblies.

The SEM image of thus-produced assemblies was measured. As shown in Figure 1C, gauzelike GO nanosheets and 1D nanostructures with a diameter of ca. 40−60 nm and a length of ca. 200−300 nm are observed. The LRTEM image of the sample (Figure 2A) reveals similar results. To disclose the internal structure of the nanorods, their HRTEM, FFT, and XRD spectra were measured. As shown in Figure 2B, distinct lattice fringes could be evidently observed from the HRTEM image, where the parallel nanostripes are aligned along the axis of the nanorods. The FFT analysis shown in Figure 2C indicates an interlattice spacing of ca. 1.55 nm. This value is very close to the diameter of ZnTPyP disk, which is calculated to be 1.56 nm.[17] Meanwhile, the XRD pattern of the samples shown in Figure 2D clearly indicates two diffraction peaks at 2θ = 5.39° and 10.76°, from which an interlattice distance of ca. 1.63 nm could be derived. This value is very close to the diameter of ZnTPyP disk and also to the interlattice spacing obtained from HRTEM and FFT (Figure 2B,C). Together with the facts observed from the UV−vis spectra shown in Figure 1A, these facts suggest that our nanorods are composed of parallel aligned columnar J-type aggregates of ZnTPyP molecules.[17,51,57] These results verify that, using GO as sheetlike surfactant, supramolecular nanorods of ZnTPyP with well-defined internal structure could be easily formulated via a SAS.

It is noteworthy that, besides the above-mentioned two diffraction peaks at 2θ = 5.39° and 10.76°, another peak at 2θ = 9.32°, corresponding to a d-spacing of ca. 0.95 nm, could also be detected. As discussed in the aftermentioned sections, this could be owing to the complexation of ZnTPyP with the locally distributed polyaromatic fragments of GO, which is induced by the $\pi-\pi$ stacking interactions between the flattened ZnTPyP and GO nanosheets.

It is widely known that the most distinguished character of SAS protocol is that a controllable self-assembly could be easily realized by means of altering the concentration of the involved surfactants.[16−30] To further confirm that GO could indeed play a role of surfactant during the assembly, similar SAS was carried out using an aqueous dispersion of GO with a higher concentration (0.02 mg mL^{-1}) as host solution (thus-obtained samples are named as Sample (0.02), hereafter). As shown in Figure 1A, after the evaporation of chloroform for 20 min, the digital photograph and UV−vis spectrum of the dispersion exhibit almost similar features as those of Sample (0.01). Interestingly, as shown in Figures 1D and 2E, the SEM and LRTEM results indicate that 1D nanostructures with a length of ca. 0.6−1.0 μm and a diameter of ca. 40−80 nm are assembled in this case. The length of these 1D nanoassemblies is distinctly longer than that of the Sample (0.01). Similarly tendency has been found in the conventional SAS process using CTAB as surfactant,[16,17] solidly confirming that GO serves as surfactant in our new SAS protocol. The internal structure of these longer 1D nanostructures has also been investigated by means of HRTEM, FFT, and XRD. As shown in Figure S1, Supporting Information, similar results as those of Sample (0.01) are obtained, suggesting that, in these longer supramolecular nanoassemblies, the ZnTPyP units are also arranged as J-type aggregates, which are aligned along the axis of the 1D nanostructures.

Practically, owing to the immiscibility of oil (chloroform) and water, an opaque emulsion system was obtained right away after the addition of a chloroform solution of ZnTPyP into the aqueous dispersion of GO nanosheets. The SAS process could thus not be well monitored in a real-time manner; although after the evaporation of the chloroform, a transparent dispersion could be obtained and the produced samples could be characterized by various methods. To overcome this, we carried out similar experiments using a THF solution of ZnTPyP as guest solution (designated as THF/water system, hereafter). In this case, the nice miscibility between THF and water allows us to monitor our SAS via real-time UV−vis spectra, since the assembly system manifests itself as a transparent dispersion all the time throughout the SAS period.

As shown in Figure 3A, the THF solution of ZnTPyP displays a monomeric B-band at 422 nm. In contrast, a B-band at ca. 444 nm is evidently detected immediately after the addition of the THF solution of ZnTPyP into the aqueous dispersion of GO (0.02 mg mL^{-1}). Compared with the monomeric B-band of ZnTPyP at ca. 422 nm, this band displays an evident bathochromic shift of ca. 22 nm, and no hypsochromic B-band could be clearly discerned. Silklike films but no 1D nanostructures could be observed from the SEM image of the samples (Figure 3B). These results suggest the formation of the ZnTPyP/GO complex at this stage, which is induced by the $\pi-\pi$ stacking between ZnTPyP and the locally distributed polyaromatic ring of GO.[58,59] The bathochromic shift of the B-band is owing to the flattening of ZnTPyP molecules (coplanar conformation of the pyridyl groups with the porphyrin core).[58−61] When the stirring proceeds for 5 min, the B-band of the dispersion displays a further bathochromic shift to ca. 449 nm, and a weak shoulder B-band at ca. 428 nm could also be discerned. As shown in Figure 3C, short nanorods, with a length of ca. 200−400 nm, and silklike GO nanosheets could be observed from the SEM image of the produced samples. These facts indicate that some of the initially formed ZnTPyP/GO complex disassembly and the released monomeric ZnTPyP molecules begin to form J-aggregates.

When the stirring time is extended to 20 min, the UV−vis spectrum of the dispersion exhibits a bathochromic B-band at ca. 455 nm and a hypsochromic B-band at ca. 415 nm, which is accompanied by a shoulder band at 422 nm. This spectrum is very similar to that observed from the corresponding chloroform/water system shown in Figure 1A, and such spectral feature exhibits negligible changes when the stirring time is further extended. This result indicates a further growth of the shorter nanorods formed at the former stage, leading to the formation of longer 1D nanostructures.[57] To confirm this, the SEM and LRTEM of the samples are investigated. As shown in Figure 3D,E, nanorods, with a length of ca. 1−2 μm, are observed. The length of these 1D nanostructures is longer than that of the samples produced in the former stage, confirming a further growth of these 1D nanospecies.

The HRTEM and FFT of these 1D nanostructures are shown in Figure S2A,B, Supporting Information, respectively. Similar results as those of the 1D nanospecies formulated in the chloroform/water systems are observed, indicating that, when a THF solution of ZnTPyP is employed as the guest solution, the as-assembled 1D supramolecular nanostructures also have a well-defined internal structure. Simultaneously, in analogous to the XRD pattern of the samples obtained in the chloroform/water systems (Figures 2D and S1C, Supporting Information), we note that, in addition to the two diffraction peaks (2θ = 5.39° and 10.76°) ascribing to the ZnTPyP 1D nanostructures, another peak at 2θ = 9.32°, corresponding to a d-spacing of ca. 0.95 nm, could also be detected from these samples (Figure S2C, Supporting Information). To elucidate this issue, the XRD spectra of our original GO nanosheets were measured, wherein a diffraction peak at 2θ = 12.1°, indicating a d-spacing of ca. 0.73 nm, was observed (Figure S3, Supporting Information). This suggests that the above-mentioned diffraction peak of the samples indicative of a d-spacing of ca. 0.95 nm could not be ascribed to our GO nanosheets. As known, the thickness of the polyaromatic ring of graphene and of porphyrin is both ca. 0.34 nm. This d-spacing of ca. 0.95 nm is very close to 3 × 0.34 nm, suggesting that this peak is attributed to the $\pi-\pi$ stacking induced ZnTPyP/GO complexes, wherein the flattened ZnTPyP molecules are lying on the polyaromatic segments of GO nanosheets.

Our SAS was also carried out in the THF/water system using a GO aqueous dispersion of a lower concentration (0.01 mg mL^{-1}) as the host solution. As shown in Figure S4, Supporting Information, shorter 1D nanostructures with a length of ca. 300−500 nm are formulated in this case. The internal structural features of these nanoassemblies are similar to those of the longer ones (Figure S5, Supporting Information). These results suggest that 1D supramolecular nanoassemblies with controlled length could be also achieved in the THF/water system, further confirming that GO plays a role of surfactant during our GO-based SAS procedure.

On the basis of the experimental facts, a plausible interpretation could be proposed for our interesting results, as schematically illustrated in Scheme 1C. Upon the introduction of ZnTPyP molecules into an aqueous dispersion of GO, ZnTPyP molecules are first captured by the two-dimensional sheetlike GO surfactants, leading to the formation of ZnTPyP/GO complex, which is driven by the $\pi-\pi$ stacking interactions between the locally distributed polyaromatic ring of GO nanosheets and the flattened ZnTPyP molecules.[58,59] In

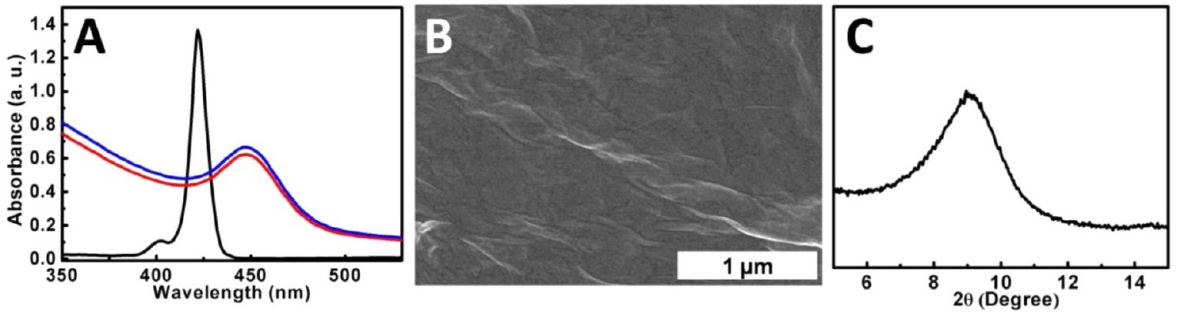

Figure 4. (A) UV−vis spectra of the samples assembled in the THF/water system, wherein an aqueous dispersion of GO with a concentration of 0.1 mg mL^{-1} was used as the host solution. The stirring time is 0 min (red curve) and 5 months (blue curve), respectively. That of ZnTPyP dissolved in THF solution (black curve) is also presented for comparison. SEM image (B) and XRD pattern (C) of the as-formulated samples.

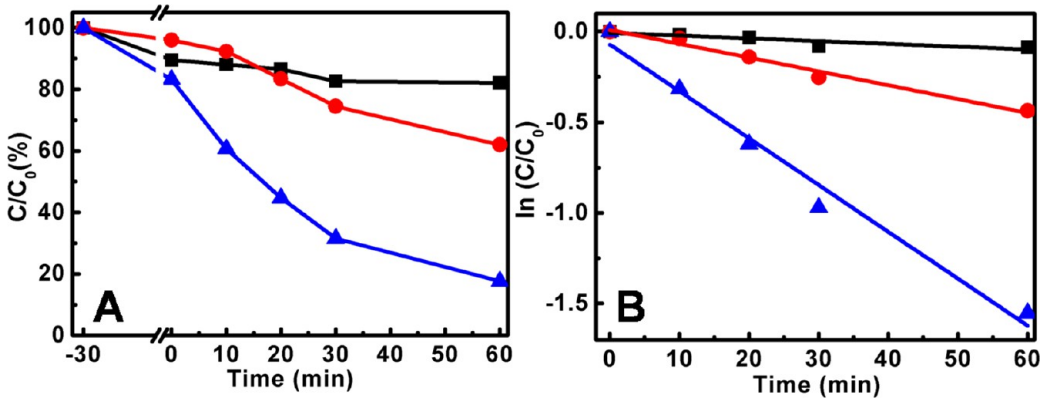

Figure 5. Photocatalytic activity (A) and kinetic linear simulation curve (B) of the original GO nanosheets (black ■), 1D ZnTPyP nanoassemblies formulated via the CTAB-assisted (red ●) and GO-assisted (blue ▲) SAS, for the photodegradation of RhB under visible-light irradiation. Prior to catalytic performance, a dark adsorption experiment was performed to achieve an equilibrium adsorption state. See Figure S6, Supporting Information, for the results of other control experiments.

these complexes, ZnTPyP molecules adopt a coplanar conformation.[58−61] This could be verified by the nonsplitting but evidently bathochromically-shifted B-band of the samples formulated at this stage (Figure 3A). With the progress of the assembly, some of the initially formed ZnTPyP/GO disassembly and simultaneously the released ZnTPyP began to aggregate, leading to the formation of shorter 1D nanostructures, which are composed of J-type supramolecular assemblies of ZnTPyP. This could be supported by the further bathochromically-shifted and gradually split B-band and the shorter 1D nanospecies observed at this stage (Figure 3A,C). With the further progress of the assembly, the shorter 1D nanostructures formed at the former stage work as template to induce other ZnTPyP released by ZnTPyP/GO complex to grow, resulting in the formation of longer 1D nanospecies.[57] This could be verified by the distinctly split B-bands and the longer 1D nanostructures observed at this stage (Figure 3A,D,E).

It thus could be seen that the complexation of ZnTPyP with the two-dimensional sheetlike GO surfactants plays an important role during this kind of GO-assisted SAS procedure. ZnTPyP is nearly a water-insoluble compound, while GO could be well dispersed in water. On the basis of these understandings and the proposed explanation (Scheme 1C), it is reasonable to expect that only ZnTPyP/GO but negligible 1D ZnTPyP nanoassemblies could be produced when a more concentrated aqueous dispersion of GO is employed during the assembly, since a higher GO concentration favors the formation of ZnTPyP/GO complexes but disfavors the aggregate of ZnTPyP itself. To validate this, we performed our SAS using a 0.1 mg mL^{-1} aqueous dispersion of GO as the host solution. As shown in Figure 4A, the UV−vis spectra of the obtained dispersion display a bathochromically-shifted B-band at ca. 447 nm, and importantly, this spectral feature displays no further changes even when the dispersion was kept for 5 months. Meanwhile, no 1D nanoassemblies but silklike films could be observed from the SEM image of thus-formulated samples (Figure 4B), whose XRD pattern displays a diffraction peak at $2\theta = 9.1°$, indicating a d-spacing of ca. 0.97 nm (Figure 4C). This value is larger than that of our original GO nanosheets (Figure S3, Supporting Information) but very close to 3 × 0.34 nm. These interesting experimental results suggest the formation of $\pi-\pi$ stacking induced ZnTPyP/GO complex, where the flattened ZnTPyP molecules are lying on the polyaromatic segments of GO nanosheets, verifying our explanations shown in Scheme 1.

3.2. Photocatalytic Performance of the One-Dimensional ZnTPyP Nanostructures Assisted by GO for the Photodegradation of RhB under Visible-Light Irradiation. We recently show that the 1D ZnTPyP nanospecies via the conventional CTAB-assisted SAS could work as organic photosemiconductors for a photocatalytic degradation of RhB.[51] As a preliminary example to demonstrate the advantage of our GO-assisted SAS, the photocatalytic behavior of Sample (0.02) of the chloroform/water system was studied, wherein the content of the 1D ZnTPyP nanostructures was about 0.1 mg. As shown in Figure S6, Supporting Information, for the blank experiment without photocatalyst, negligible degradation of RhB molecules could be observed, suggesting that the self-

sensitized photodegradation of RhB could hardly occur under our experimental conditions. As shown in Figure 5, GO itself displays negligible catalytic effect, although it could adsorb RhBs. When the 1D nanostructures via the CTAB-assisted SAS are used,[51] ca. 38% RhBs are decomposed, and the rate constant of the reaction is ca. 7.6×10^{-3} min^{-1}. In contrast, when those via the GO-assisted SAS are used, evident RhB adsorption is observed, and ca. 83% RhBs are decomposed under the similar experimental conditions. The rate constant in this case is ca. 2.6×10^{-2} min^{-1}. These facts indicate that, compared with those assembled via the conventional CTAB-assisted SAS, the 1D nanospecies constructed via our present GO-assisted SAS could display distinctly enhanced catalytic performances.

Moreover, as shown in Figures 5 and S6, Supporting Information, the photocatalytic activity of the Sample (0.02) of the chloroform/water system is much higher than that of the commercially available P25–TiO_2, whose rate constant under our experimental conditions is estimated to be ca. 2.9×10^{-3} min^{-1}. For comparison, the photocatalytic performance of the ZnTPyP/GO complexes fabricated at high concentration of GO (0.1 mg mL^{-1}) was also carried out, as shown in Figure S6, Supporting Information. It can be seen that, compared with the photocatalytic behavior of Sample (0.02), these ZnTPyP/GO complexes display evidently larger adsorption capacity (ca. 32%) to RhB molecules. However, they exhibit very low catalytic performance in their catalytic behavior (4.7×10^{-3} min^{-1},) which is substantially lower than that of Sample (0.02). As a matter of fact, this is in good agreement with our previous observations, wherein it has been proved that the 1D ZnTPyP nanoassemblies could work as organic photosemiconductors for a photocatalytic degradation of RhB, since their J-aggregates in the 1D structure faciliates the electron transfer process, leading to a distinct photocatalytic performance. In contrast, the monomeric state of ZnTPyP disfavors the electron transfer process, resulting in a low photocatalytic activity.[51]

As known, GO is currently recognized to be ideal catalyst support or promoter, owing to its unique physicochemical properties.[50,62−67] Numerous GO-hybridized inorganic-based catalysts with boosted catalytic activity have been constructed,[50,62−65] where the facilitated charge transfer and the suppressed recombination of electron−hole pairs and the promoted adsorption of the substrate molecules, which are aroused by GO, are suggested to play an important role.[50,62−65] To preliminarily disclose the higher catalytic performance of our 1D ZnTPyP supramolecular nanoassemblies assisted by GO, their EIS spectra were investigated as Nyquist plots, as shown in Figure 6A. It can be seen that the size of the arc radius of the GO-assisted 1D ZnTPyP nanoassemblies is distinctly smaller than that of the CTAB-assisted 1D nanostructures. This suggests a decrease in the solid state interface layer resistance and the charge transfer resistance on the surface of our GO-assisted 1D nanostructures,[68] and it indicates that the presence of GO nanosheets might promote the charge transfer and thus suppress the recombination of the photogenerated electron−hole pairs, leading to an enhance catalytic peroformance.[50,52,69]

As is known, the Raman spectrum is a powerful probe for exploring the electronic structure of graphene-based nanomaterials, wherein the characterized position of the G-band of GO nanosheets is among the most frequently mentioned issues. Practically, the occurrence of charge transfer between GO and the hybridized components could be verified by the Raman spectra, wherein it has been demonstrated that the G-band of

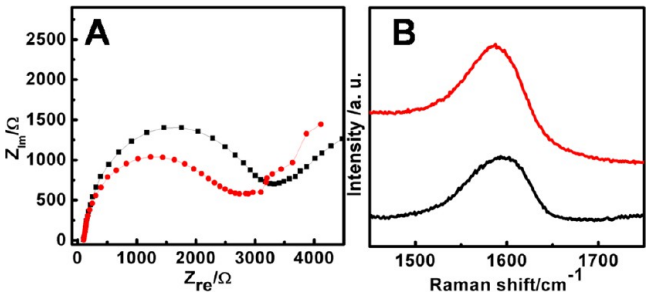

Figure 6. (A) EIS spectra of the film electrodes of the 1D ZnTPyP nanostructures formulated with the assistance of CTAB (black curve) and GO (red curve). (B) Typical Raman spectra of the G-band of our original powdery GO nanosheets (black curve) and Sample (0.02) (red curve) formulated in the chloroform/water system.

GO nanosheets shifts to lower frequency (softening) when GO is hybridized with an electron donor component. In contrast, the G-band would shift to a higher frequency (stiffening) when an electron acceptor component is hybridized.[50,52,70−73] For examples,[50,52,69] in terms of Raman spectra, we have recently identified the occurrence of charge transfer from silver/silver halide nanospecies to GO nanosheets, wherein it was found that GO facilitated the charge separation in silver/silver halide and thus promoted the catalytic performance of the silver/silver halide species.

It has been previously reported that electron transfer could occur between aromatic molecules and GO nanosheets.[74] In our present case, to further prove the occurrence of the charge transfer between our 1D ZnTPyP nanostructures and GO nanosheets experimentally, the Raman spectrum of Sample (0.02) formulated in the chloroform/water system together with that of the original powdery GO nanosheets was measured, as shown in Figure 6B. It can be seen that a G-band at ca. 1598 cm^{-1}, which is a typical Raman feature of GO nanosheets, could be observed from our original powdery GO. In contrast, the G-band shifts by 11 cm^{-1} to a lower frequency of ca. 1587 cm^{-1} in the case of the Sample (0.02). Together with the experimental facts derived from the EIS investigation (Figure 6A), these results confirm the occurrence of charge transfer between the GO nanosheets and the 1D ZnTPyP nanostructures of Sample (0.02), wherein the former (GO nanosheets) and latter (1D ZnTPyP nanostructures) work as electron-acceptor and electron-donor components, respectively. As a result, the electrons originally photogenerated in the 1D ZnTPyP supramolecular photosemiconductors could migrate into GO nanosheets through a percolation process[50,52,70−73] during the photocatalytic performance, promoting the charge separation/transfer, and thus suppress the recombination of electron−hole pairs in the 1D ZnTPyP nanostructures, resulting in an enhancement of the photocatalytic performance.[50,52,70−73] On the other hand, it can be seen from Figure 5A that, compared with the 1D nanostructures assisted by CTAB, those assisted by GO nanosheets display a much higher adsorptive capacity to RhB molecules. This could be owing to the presence of GO nanosheets in this system, which might also contribute partially to the observed enhance photocatalytic activities.[50,52,69,75]

4. CONCLUSIONS

In summary, we have demonstrated that GO could play a role of a 2D sheetlike surfactant for the controllable assembly of 1D

supramolecular nanostructures of a porphyrin with well-defined internal structure. In terms of SAS, which is a nanofabrication strategy of general concern, our investigation discloses a new facet of the amphiphilic sheetlike GO surfactant. The complexation of ZnTPyP with the two-dimensional GO nanosheets plays an important role in this new type of SAS, wherein GO not only works as a sheetlike surfactant in the assembly step but also serves as functional components during the catalytic performance of the formulated nanostructures. Great expectations might be provoked for GO nanosheets in the feild of functional supramolecular nanomaterials.

■ ASSOCIATED CONTENT

Ⓢ Supporting Information

SEM, LRTEM, HRTEM, and FFT of some of our samples assembled by our GO-assisted SAS, and the XRD pattern of our original powdery GO nanosheets, and the catalytic performances without catalysts, or using our original GO nanosheets, the ZnTPyP/GO complexes formulated at a high concentration of GO (0.1 mg mL^{-1}), and the commercially available P25–TiO_2, as catalysts. This material is available free of charge via the Internet at http://pubs.acs.org.

■ AUTHOR INFORMATION

Corresponding Author

*E-mail: chenpl@iccas.ac.cn, cpl@zzu.edu.cn (P.C.); liumh@iccas.ac.cn (M.L.). Fax: (+) 86-10-62569564. Tel: (+) 86-10-82615803.

Notes

The authors declare no competing financial interest.

■ ACKNOWLEDGMENTS

The authors acknowledge the financial support from National Natural Science Foundation of China (20873159, 21021003, and 91027042), National Key Basic Research Project of China (2011CB932301 and 2013CB834504), and CAS (1731300500015). Dr. Penglei Chen thanks Zhengzhou University for the "Talent Project of Distinguished Professor".

■ REFERENCES

(1) Lindoy, L. F.; Atkinson, I. M. *Self-Assembly in Supramolecular Systems*; Stoddart, J. F., Ed.; Royal Society of Chemistry: Cambridge, 2000.
(2) Pelesko, J. A. *Self Assembly: The Science of Things That Put Themselves Together*, 1st ed.; Chapman & Hall/CRC: Boca Raton, FL, 2007.
(3) Lehn, J.-M. *Science* **2002**, *295*, 2400–2403.
(4) Service, R. F. *Science* **2001**, *293*, 782–785.
(5) Reinhoudt, D. N.; Crego-Calama, M. *Science* **2002**, *295*, 2403–2407.
(6) Zang, L.; Che, Y.; Moore, J. S. *Acc. Chem. Res.* **2008**, *41*, 1596–1608.
(7) Scanlon, S.; Aggeli, A. *Nano Today* **2008**, *3*, 22–30.
(8) Toksöz, S.; Guler, M. O. *Nano Today* **2009**, *4*, 458–469.
(9) Greiner, A.; Wendorff, J. H. *Adv. Polym. Sci.* **2008**, *219*, 107–171.
(10) Liu, H.; Xu, J.; Li, Y.; Li, Y. *Acc. Chem. Res.* **2010**, *43*, 1496–1508.
(11) Zhou, Y.; Yan, D. *Chem. Commun.* **2009**, 1172–1188.
(12) Hirst, A. R.; Escuder, B.; Miravet, J. F.; Smith, D. K. *Angew. Chem., Int. Ed.* **2008**, *47*, 8002–8018.
(13) Palmer, L. C.; Stupp, S. I. *Acc. Chem. Res.* **2008**, *41*, 1674–1684.
(14) Lim, Y.-B.; Moon, K.-S.; Lee, M. *Chem. Soc. Rev.* **2009**, *38*, 925–934.
(15) Yan, Y.; Lin, Y.; Qiao, Y.; Huang, J. *Soft Matter* **2011**, *7*, 6385–6398.
(16) Hu, J.-S.; Guo, Y.-G.; Liang, H.-P.; Wan, L.-J.; Jiang, L. *J. Am. Chem. Soc.* **2005**, *127*, 17090–17095.
(17) Qiu, Y.; Chen, P.; Liu, M. *J. Am. Chem. Soc.* **2010**, *132*, 9644–9652.
(18) Bai, F.; Sun, Z.; Wu, H.; Haddad, R. E.; Coker, E. N.; Huang, J. Y.; Rodriguez, M. A.; Fan, H. *Nano Lett.* **2011**, *11*, 5196–5200.
(19) Shi, N.; Xie, L.; Sun, H.; Duan, J.; Yin, G.; Xu, Z.; Huang, W. *Chem. Commun.* **2011**, *47*, 5055–5057.
(20) Jang, J.; Oh, J. H. *Adv. Mater.* **2003**, *15*, 977–980.
(21) Zhang, X.; Zhang, X.; Shi, W.; Meng, X.; Lee, C.; Lee, S. *J. Phys. Chem. B* **2005**, *109*, 18777–18780.
(22) Lee, S. J.; Hupp, J. T.; Nguyen, S. T. *J. Am. Chem. Soc.* **2008**, *130*, 9632–9633.
(23) Hasobe, T.; Sandanayaka, A. S. D.; Wada, T.; Araki, Y. *Chem. Commun.* **2008**, 3372–3374.
(24) Gong, X.; Milic, T.; Xu, C.; Batteas, J. D.; Drain, C. M. *J. Am. Chem. Soc.* **2002**, *124*, 14290–14291.
(25) Lin, C.; Zhu, W.; Yang, H.; An, Q.; Tao, C.; Li, W.; Cui, J.; Li, Z.; Li, G. *Angew. Chem., Int. Ed.* **2011**, *50*, 4947–4951.
(26) Qi, L. *Coord. Chem. Rev.* **2010**, *254*, 1054–1071.
(27) Nadagouda, M. N.; Speth, T. F.; Varma, R. S. *Acc. Chem. Res.* **2011**, *44*, 469–478.
(28) Donegá, C.; Ade, M. *Chem. Soc. Rev.* **2011**, *40*, 1512–1546.
(29) Dong, R.; Liu, W.; Hao, J. *Acc. Chem. Res.* **2012**, *45*, 504–513.
(30) Xiao, J.; Qi, L. *Nanoscale* **2011**, *3*, 1383–1396.
(31) Che, Y.; Datar, A.; Balakrishnan, K.; Zang, L. *J. Am. Chem. Soc.* **2007**, *129*, 7234–7235.
(32) Reese, C.; Bao, Z. *Mater. Today* **2007**, *10*, 20–27.
(33) Zhang, Y.; Chen, P.; Jiang, L.; Hu, W.; Liu, M. *J. Am. Chem. Soc.* **2009**, *131*, 2756–2757.
(34) Jiang, L.; Fu, Y.; Li, H.; Hu, W. *J. Am. Chem. Soc.* **2008**, *130*, 3937–3941.
(35) Drain, C. M.; Varotto, A.; Radivojevic, I. *Chem. Rev.* **2009**, *109*, 1630–1658.
(36) Carlsen, C. U.; Møller, J. K.S.; Skibsted, L. H. *Coord. Chem. Rev.* **2005**, *249*, 485–498.
(37) Medforth, C. J.; Wang, Z. C.; Martin, K. E.; Song, Y. J.; Jacobsen, J. L.; Shelnutt, J. A. *Chem. Commun.* **2009**, 7261–7277.
(38) Balaban, T. S. *Acc. Chem. Res.* **2005**, *38*, 612–623.
(39) Wasielewski, M. R. *Acc. Chem. Res.* **2009**, *42*, 1910–1921.
(40) Miyatake, T.; Tamiaki, H. *Coord. Chem. Rev.* **2010**, *254*, 2593–2602.
(41) Wan, X.; Huang, Y.; Chen, Y. *Acc. Chem. Res.* **2012**, *45*, 598–607.
(42) Dreyer, D. R.; Park, S.; Bielawski, C. W.; Ruoff, R. S. *Chem. Soc. Rev.* **2010**, *39*, 228–240.
(43) Bai, H.; Li, C.; Shi, G. *Adv. Mater.* **2011**, *23*, 1089–1115.
(44) Kim, J.; Cote, L. J.; Huang, J. *Acc. Chem. Res.* **2012**, *45*, 1356–1364.
(45) Cote, L. J.; Kim, J.; Tung, V. C.; Luo, J.; Kim, F.; Huang, J. *Pure Appl. Chem.* **2011**, *83*, 95–110.
(46) Cote, L. J.; Kim, J.; Zhang, Z.; Sun, C.; Huang, J. *Soft Matter* **2010**, *6*, 6096–6101.
(47) Luo, J.; Cote, L. J.; Tung, V. C.; Tan, A. T. L.; Goins, P. E.; Wu, J.; Huang, J. *J. Am. Chem. Soc.* **2010**, *132*, 17667–17669.
(48) Kim, J.; Cote, L. J.; Kim, F.; Yuan, W.; Shull, K. R.; Huang, J. *J. Am. Chem. Soc.* **2010**, *132*, 8180–8186.
(49) Hummers, W. S.; Offeman, R. E. *J. Am. Chem. Soc.* **1958**, *80*, 1339.
(50) Zhu, M.; Chen, P.; Liu, M. *ACS Nano* **2011**, *5*, 4529–4536.
(51) Guo, P.; Chen, P.; Ma, W.; Liu, M. *J. Mater. Chem.* **2012**, *22*, 20243–20249.
(52) Zhu, M.; Chen, P.; Liu, M. *J. Mater. Chem.* **2012**, *22*, 21487–21494.
(53) Zhu, M.; Chen, P.; Ma, W.; Lei, B.; Liu, M. *ACS Appl. Mater. Interfaces* **2012**, *4*, 6386–6392.
(54) Kano, H.; Kobayashi, T. *J. Chem. Phys.* **2002**, *116*, 184–195.

(55) van Esch, J. H.; Feiters, M. C.; Peters, A. M.; Nolte, R. J. M. *J. Phys. Chem.* **1994**, *98*, 5541−5551.
(56) Kasha, M.; Rawls, H. R.; Ashraf El-Bayoumi, M. *Pure Appl. Chem.* **1965**, *11*, 371−392.
(57) Guo, P.; Chen, P.; Liu, M. *Langmuir* **2012**, *28*, 15482−15490.
(58) Xu, Y.; Zhao, L.; Bai, H.; Hong, W.; Li, C.; Shi, G. *J. Am. Chem. Soc.* **2009**, *131*, 13490−13497.
(59) Wojcik, A.; Kamat, P. V. *ACS Nano* **2010**, *4*, 6697−6706.
(60) Ishida, Y.; Masui, D.; Shimada, T.; Tachibana, H.; Inoue, H.; Takagi, S. *J. Phys. Chem. C* **2012**, *116*, 7879−7885.
(61) Wang, L.-F.; Meng, X.-W.; Tang, F.-Q. *J. Mol. Struct.: THEOCHEM* **2010**, *956*, 26−32.
(62) Xiang, Q.; Yu, J.; Jaroniec, M. *Chem. Soc. Rev.* **2012**, *41*, 782−796.
(63) An, X.; Yu, J. C. *RSC Adv.* **2011**, *1*, 1426−1434.
(64) Machado, B. F.; Serp, P. *Catal. Sci. Technol.* **2012**, *2*, 54−75.
(65) Huang, C.; Li, C.; Shi, G. *Energy Environ. Sci.* **2012**, *5*, 8848−8868.
(66) Min, S.; Lu, G. *J. Phys. Chem. C* **2011**, *115*, 13938−13945.
(67) Mou, Z.; Dong, Y.; Li, S.; Du, Y.; Wang, X.; Yang, P.; Wang, S. *Int. J. Hydrogen Energy* **2011**, *36*, 8885−8893.
(68) Zhang, H.; Lv, X.; Li, Y.; Wang, Y.; Li, J. *ACS Nano* **2010**, *4*, 380−386.
(69) Zhu, M.; Chen, P.; Liu, M. *Langmuir* **2012**, *28*, 3385−3390.
(70) Xu, Y.; Wu, Q.; Sun, Y.; Bai, H.; Shi, G. *ACS Nano* **2010**, *4*, 7358−7362.
(71) Ghosh, A.; Rao, K. V.; George, S. J.; Rao, C. N. R. *Chem.—Eur. J.* **2010**, *16*, 2700−2704.
(72) Das, A.; Pisana, S.; Chakraborty, B.; Piscanec, S.; Saha, S. K.; Waghmare, U. V.; Novoselov, K. S.; Krishnamurthy, H. R.; Geim, A. K.; Ferrari, A. C.; Sood, A. K. *Nat. Nanotechnol.* **2008**, *3*, 210−215.
(73) Geng, J.; Jung, H.-T. *J. Phys. Chem. C* **2010**, *114*, 8227−8234.
(74) Ramakrishna, M. H. S. S.; Subrahmanyam, K. S.; Venkata, R. K.; George, S. J.; Rao, C. N. R. *Chem. Phys. Lett.* **2011**, *506*, 260−264.
(75) Zhu, M.; Chen, P.; Liu, M. *Chin. Sci. Bull.* **2013**, *58*, 84−91.